Research Article | Vol. 29, No. 11 / 24 May 2021 / Optics Express 15906
Optics EXPRESS

High sensitivity static Fourier transform spectrometer

FABIO FRASSETTO,[1,2,*] LORENZO COCOLA,[1,2] PAOLA ZUPPELLA,[1] VANIA DA DEPPO,[1] AND LUCA POLETTO[1]

[1] CNR-IFN Padova, Via Trasea 7, 35131 Padova, Italy
[2] Both authors have contributed equally to this study
[*] fabio.frassetto@cnr.it

Abstract: Static Fourier transform spectrometers (S-FTSs) are well-consolidated instruments providing high throughput and high spectral resolution in a narrow spectral band. They use two reflective gratings as dispersive elements in a Michelson interferometer. Gratings allow high spectral dispersion and consequently high resolution, but, due to the light diffused from their grooves, they are one of the main noise sources in the reconstructed spectrum. In this work, we compare the signal-to-noise ratio performance of a prism-based S-FTS with that of a grating-based S-FTS. As a primary advantage, prisms give intrinsically lower diffused light than gratings. Furthermore, they do not have multiple diffracted orders, reducing thereafter the optical constraints on the instrumental baffling.

1. Introduction

Three parameters are primarily used to describe a spectrometer: resolution, signal to noise ratio and throughput. Which one needs to be maximized depends on the particular application case. There are many applications, either scientific or industrial, where the high-resolution capability of spectrographs is not strictly required and it is desirable to improve the performance of the instrumental throughput and the signal to noise ratio [1–4]. Here we propose a design concept for the realization of spectrometers using Static Fourier transform spectroscopy with high signal to noise ratio and high throughput in the visible spectral region [5].

The physical part of a Static Fourier transform spectrometer (S-FTS) is an interferometer in which a static interference pattern is recorded via a two-dimensional detector. This signal, the so-called interferogram, is processed to obtain the spectrum. The Wiener–Khintchine theorem [6,7] connects the autocorrelation of a signal to its power spectrum via the Fourier transform operator [8,9].

The first proposal of what today is referred to as S-FTS dates back to the work of Connes [10] in 1958. Two years later, in a note in parentheses, Jacquinot [11] reported that the mirrors in the Michelson interferometer in the Connes' work could be replaced with (cit.) "*reflection gratings, prisms with a reflecting face or more complex combinations of prisms and gratings*". To our knowledge, no following developments of this technique were proposed in the literature until Harlander [12,13], in the '90s, rediscovered the idea of using gratings in a Michelson interferometer. Starting from the systematic research of Harlander, S-FTS instruments have been based on the use of reflective diffraction gratings [14–17]. These optical devices are one of the main sources of noise in the reconstructed spectrum, due to the stray-light produced by the micro-roughness of each groove [18].

In order to increase the signal to noise (S/N) ratio, we discuss in this paper the substitution of gratings with prisms in Littrow [19] configuration, following the suggestion in the paper from Jacquinot. The Jacquinot considerations are based on the use of "*prisms with a reflecting face*" as an alternative way to produce the wavefront dispersion. However, the beneficial effects that this substitution has on the S/N of the reconstructed interferogram were not discussed. To the

#422645 https://doi.org/10.1364/OE.422645
Journal © 2021 Received 15 Feb 2021; revised 30 Mar 2021; accepted 31 Mar 2021; published 10 May 2021

Optics EXPRESS

authors' knowledge, the capabilities and peculiarities of this kind of instrument have never been deeply studied. In particular, for demanding applications such as astronomical observations of extended faint objects, the availability of low noise detectors can confine the dominant source of noise from the electronic hardware to the optical equipment. In this scenario, the idea of using low roughness optical elements can be of interest in the situations where moderate resolution is required and in spectral regions where glasses can be used as dispersive elements.

Furthermore, gratings, whereas blazed and used at Littrow incidence angle, produce multiple diffraction orders. In order to avoid the corruption of the interferogram caused from those spurious contributions, an appropriate baffling system needs to be designed [20] and in some cases this baffling system can be only partially effective, due to the instrumental constraints (bandpass, luminosity, resolution etc.).

The main advantage of using prisms is the reduction of diffused light, since prisms can be manufactured with a higher optical quality than gratings over a large optical surface. Another advantageous effect of the use of prisms is the absence of multiple diffraction orders and a more uniform transfer efficiency inside the working spectral band. Both these aspects guarantee the reduction of the noise in the interferogram.

Depending on the particular considered application for the instrument, either stray-light or undesired diffracted light could be the dominant effect.

The use of prisms as (pure) dispersive elements permits to disentangle the splitting and recombination processes from the dispersive one, this last driving the instrumental resolution.

It is worth mentioning that prisms are already used as beam splitters in a different class of S-FTSs based on the use of the Wollaston configuration [21,22]. The working principle of those instruments is driven by the different path that the light experiences at different polarization states. The collinear geometry of the two arms in the interferometer permits to obtain extremely compact spectrometers, but this requires the use of two polarization plates.

Also in the case in which Wollaston prisms are used there are no dedicated dispersive elements in the optical layout.

Lastly, some instruments [23,24] use no dispersion at all between the interferometer arms; in this case, the dependence of the fringe pattern on the wavelength itself can be used to detect "low" resolution static spectra.

The paper is divided in six sections as hereafter described. In the introduction, a historical background on the basic principles of the S-FTS spectroscopy is briefly illustrated. In the second section the principles of the optical layout are given, while in the third section the analytical aspects of the technique are presented. In section four the optical set-up, used in the experiment, is described. In section five the morphological measures to assess the optical quality (roughness and waviness) of the two used optical elements are given and the experimental results, obtained using the gratings and prisms setups, are showed and explained.

2. Optical layout - background

Two ideally monochromatic beams produce a time-invariant spatial energy distribution in the region of space where they overlap: the interferogram. To help the reader to visualize the phenomenon, in Fig. 1 the interference process of two monochromatic beams is represented. Considering two monochromatic coplanar collimated beams of wavelength λ with an angle of 2γ, the interferogram, on a plane orthogonal to the bisector of the two beams, is characterized by a spatial frequency $\nu = \frac{1}{d} = \frac{2\,sin\gamma}{\lambda}$ that depends both on γ and λ. In case of polychromatic radiation, the interferogram consists of the sum (integral) of the contribution of each spectral (infinitesimal) component.

In S-FTS, the variation in the spatial frequency of the fringes composing the interferogram is amplified, being in this case γ a function of the wavelength. This effect is produced by the dispersive elements (gratings or prisms, as proposed in this paper) present in the beam path. The

Optics EXPRESS

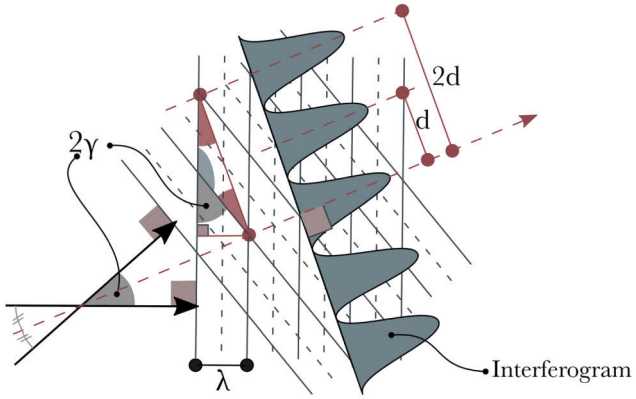

Fig. 1. Interference process of two collimated monochromatic beams. λ is the monochromatic wavelength, γ the semi-angle between the two beams and "d" the distance between two maxima in the interferogram.

variation of γ with the wavelength produces the heterodyne effect: for the monochromatic beams of wavelength λ, the spatial pattern in the interferogram depends (in first approximation) on the difference $\lambda-\lambda_L$. The λ_L represents the Littrow wavelength: the one that is retro-dispersed along the incidence direction (see the following section n. 3 for details on the Littrow wavelength). The heterodyne effect justifies the name of spatial heterodyne spectrometer/spectroscopy (SHS) sometimes used to refer to this instrument/technique.

3. Dispersive and retro-reflecting dispersive prism principles

In this section, the use of a Littrow prism as dispersive retroreflector is discussed. Figure 2 illustrates the analogies between the light path in a standard prism and in a Littrow prism with a reflective surface on the axis of symmetry of the prism. Four cases are presented: a) refracting dispersive prism layout working at a generic wavelength to be compared with b) Littrow prism generic configuration and c) refracting prism used at the minimum angle of deviation configuration to be compared with d) Littrow prism at minimum angle of deviation.

In Fig. 2, "α" is the apex angle, "*i*" the incidence angle, "*o*" the refracted emerging angle and "δ" the angular deviation, i.e. the difference between the incidence and the emerging angles, while β is 180°- α.

In the generic refraction prism configuration (a) $\delta=i+o-\alpha$ and using the Snell law the following relations can be derived:

$$\sin o = \sin\alpha\sqrt{n^2-(\sin i)^2}-\sin i\cos\alpha \tag{1}$$

$$\delta = i+\sin^{-1}\left(\sin\alpha\sqrt{n^2-(\sin i)^2}-\sin i\cos\alpha\right)-\alpha \tag{2}$$

For the minimum deviation condition $i=o$ and $\delta=2i-\alpha$, Fig. 2(c): $\sin i = n(\lambda)\sin\left(\frac{\alpha}{2}\right)$.

For the Littrow retro-reflecting dispersive prism configuration, the difference between the incidence "*i*" and real emerging direction "*o*" is $\gamma=o-i$ see Fig. 2(b)).

The dispersive element maps λ into γ(λ), and consequently into the frequency of the interferogram:

$$\gamma(\lambda) = \sin^{-1}\left(\sin\alpha\sqrt{(n(\lambda))^2-(\sin i)^2}-\sin i\cos\alpha\right)-i \tag{3}$$

where n(λ) is the refractive index expressed as a function of the wavelength λ. For the condition of minimum deviation $i=o$ γ=0 (Fig. 2(d)).

Optics EXPRESS

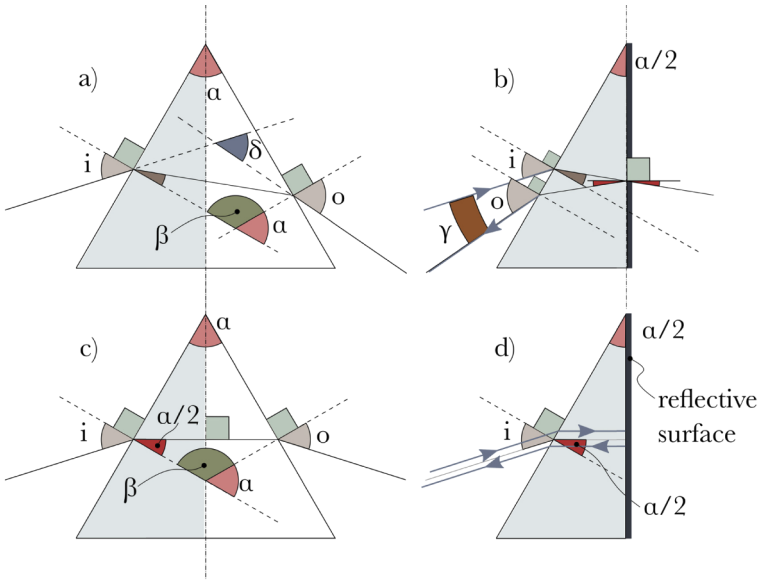

Fig. 2. Geometry analogies between the ray's refraction in a prism and the retro refraction in a Littrow prism. a) and c) refraction process (in c the minimum deviation configuration is considered). b) and d) retro-reflection and refraction processes (in d the minimum deviation configuration is considered).

For comparison, if a grating is used as retro-reflecting dispersive element in the so-called Littrow configuration, indicating with λ_L the Littrow wavelength, σ the groove density and m the diffraction order, the angular dispersion is:

$$\gamma(\lambda) = \sin^{-1}\left(m\sigma\lambda - \frac{m_L\lambda_L\sigma}{2}\right) - \sin^{-1}\left(\frac{m_L\lambda_L\sigma}{2}\right) \tag{4}$$

Compared to Eq. (3), the dispersion introduced when a grating is used (Eq. (4)) is almost linear in λ. The non-linear dispersion introduced by the prisms produces a non-linear wavelength scale in the reconstructed spectrum: this effect has to be taken into account in the data analysis process. The effect is simulated in Fig. 5.

Another aspect that makes prisms based S-FTS deeply different from the grating based ones is the spectral contamination in the reconstructed spectrum. Figure 3(a)) illustrates the angular dispersion of a 150 lines/mm grating at three different diffraction orders. The blaze wavelength is 633nm. The three brown areas indicate, for each wavelength, the maximum acceptable interfering angle (γ in Fig. 1) producing a detectable interference pattern free from aliasing (most internal region) and those γ producing patterns at higher frequency and consequently aliased in the acquisition process. The colored regions represent what the detector can "see" whilst the lines (m=0, m=-1, . . .) what the dispersive element produces. Given a generic λ, the γ interval visible at the detector plane at the different aliased levels depends on the sampling step via the Nyquist theorem. The demagnification factor considered in the calculation is M=1.8 ($M = \frac{W}{d} = \frac{p}{q}$, see Fig. 4) and the sampling interval is 5.86μm.

Wavelengths that are harmonics of the ones inside the instrumental spectral band ($\frac{\lambda}{2}, \frac{\lambda}{3}, ..$) can reach the detector (they propagate as λ) through the attenuation offered by the filter, and the other optical elements, Fig. 3(b1)). This attenuation heavily depends on the filter type used, interferential or colored glass. For a single interferential filter, offering very high rejection rate and band-pass up to hundreds of nm centered in the visible band, the typical off-band optical

Optics EXPRESS

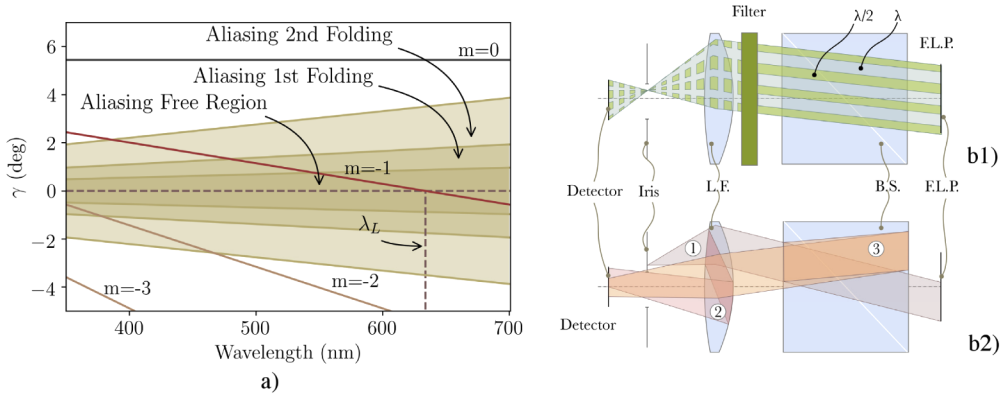

Fig. 3. a) Plot of γ(λ) for three orders of diffraction and for the specular reflection. The colored regions indicate the maximum (acceptable) angle producing detectable fringes at the detector plane, or detectable at the first and second frequency folding (aliasing). b) Two sources of noise. F.L.P. fringe localization plane, B.S. beam-splitter, L.F. focalization lens. b1) Wavelengths, harmonics of the fundamental, propagate along the same direction. The radiation that is not blocked by the filter reaches the detector. b2) A wavelength out of the detectable spectral range (path 1) can reach the detector plane via inter-reflection at the focusing lens (path 2) or at the beam-splitter (path 3).

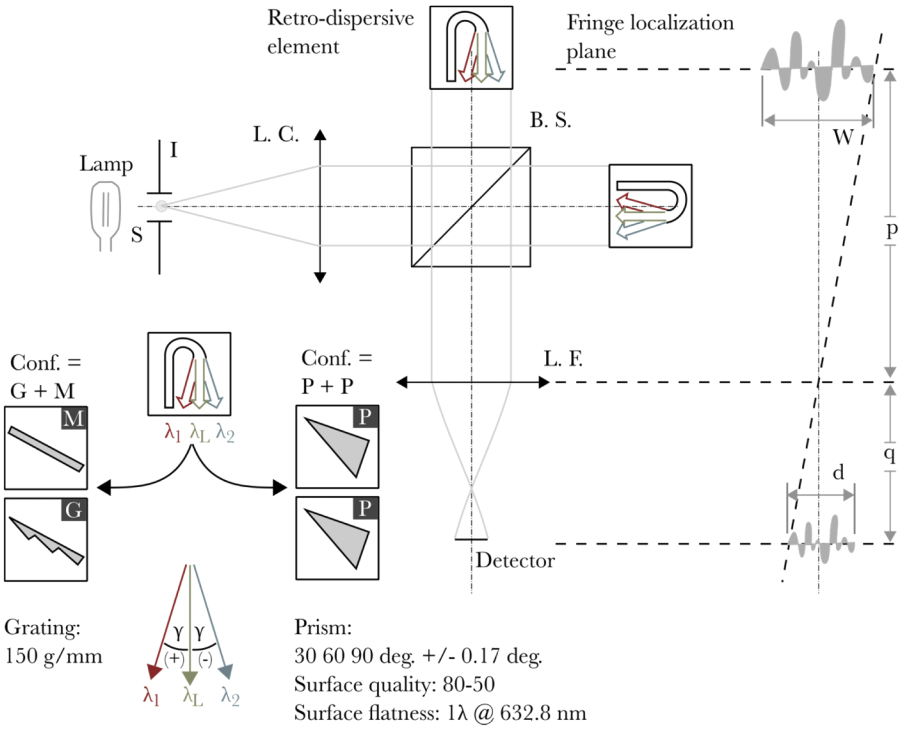

Fig. 4. Schematic of the optical set-up used for the S/N comparison. The main parameters for both the grating and prisms are listed at the bottom of the figure. The lamp illuminates the iris "I" and realizes in this way the source "S". Lengths p and q are respectively the entrance and exit arms of L. F.; W is the size of the interferogram, consequently d is the useful size of the detector.

Optics EXPRESS

density is 3 to 4. Moreover, wavelengths out of the detectable spectral range (path 1 in Fig. 3(b2)) can reach the detector plane via inter-reflection at the focusing lens (path 2 in Fig. 3(b2)) or at the beam-splitter (path 3 in Fig. 3(b2)). This effect is also present if prisms are used, but is emphasized when multiple diffraction orders are generated by gratings.

4. Experimental optical setup

With the purpose of highlighting the noise reduction in the reconstructed spectrum when prisms are used in place of diffraction gratings, the set-up schematically shown in Fig. 4 has been realized.

In order to compare two instruments of similar resolving power, the usual two-grating layout has been modified in one having a grating in one arm and a flat mirror in the other. Using the single-grating configuration, the spectral resolution of the two instruments that we compare is similar and the signal to noise performance of the grating-based version is increased, since one of the two optical elements is a mirror. Therefore, the prism-based configuration is compared with a grating-based version featuring the least amount of noise. This configuration, indicated here after as "Conf. G + M", is compared with the prism-based variant (with two prisms) and indicated as "Conf. P + P".

Both the grating and prisms are commercially available components. The prisms (Edmund Optics 43-673) are 30°-60°, aluminum coated N-BK7 with a surface flatness of 1λ @ 632.8nm.

The grating (Edmund Optics 64-402) used for the S/N comparison is a ruled (replica) with 150 lines/mm, blaze angle 2.13° and coated with *bare aluminum*. Coupled with a flat mirror, the grating produces an angular dispersion almost equal to the one introduced by the prisms, see Fig. 5.

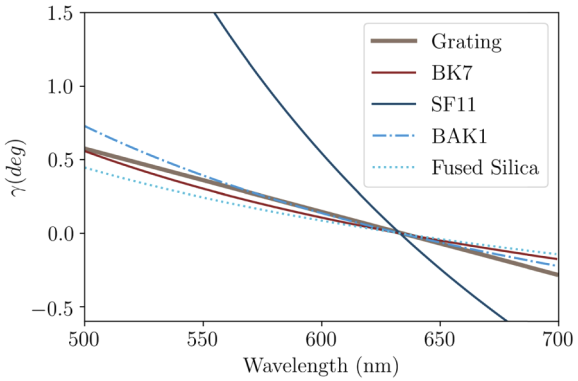

Fig. 5. Angular deviation, γ(λ), of the dispersed radiation in case of a 150 gr/mm grating and a flat mirror, or a couple of prisms made of different glasses. λ_L=632.8 nm.

The test lamps are Philips spectral lamps (low-pressure, discharge) model 93101 filled with Kr and 93103 filled with K. The collimating lens, L. C., is a photographic objective with focal length of 50mm. The used detector is a Basler acA1920-40gm, featuring a 1920 × 1200 CMOS sensor with a 5.86μm pixel pitch, featuring 12bit ADC conversion. The Fringe Localization Plane (F. L. P.) is imaged on the focal plane array with a Pentax 50mm, f/# 1.8 TV lens. The beam diameter after L. C. is 20mm.

The retro-dispersive element, one for each arm, represents the key functioning principle of both gratings and prisms: a specific wavelength (λ_L) is diffracted/refracted along the same direction along which all the wavelengths emerge from the beam-splitter; for $\lambda \neq \lambda_L$ the radiation is redirected to the detector forming an angle $\gamma(\lambda-\lambda_L)$ with the optical axis. In Fig. 4 the

Optics EXPRESS

retro-dispersive element is also used to represent the degenerate case in which a mirror is used. In this case the angle γ is independent from the wavelength.

Figure 5 shows the comparison of the dispersion angle γ(λ) for the single-grating configuration (150 gr/mm groove density) and for a couple of prisms made of different glasses. The incidence angle used for the prisms is i_{BK7}=49.2°, i_{SF11}=62.78°, i_{BAK1}=51.73°, $i_{FUS.\ SIL.}$=46.76°. All the incidence angles are calculated supposing α=60°.

The use of different glasses produces, inside the considered spectral band, different values of the angular dispersion. Figure 5, in particular, emphasizes the change in the angular dispersion when a low dispersion glass (BK7, BAK1 or fused silica) is compared with a high dispersion glass (SF11). The glass type used in the prisms introduces a freedom degree useful to tune the spectrometer parameters (resolution and bandpass) to the particular application. No A/R coating has been adopted in the proposed setup although, with such large values of "i", the use of a custom antireflection coating on the prism may be recommended. This was determined by the prisms available at the time the experiment was carried out. It is worth to note that the absence of an A/R coating can produce only deteriorating effects, and consequently, the results we found can be only beneficially affected by the introduction of A/R coatings.

The integration time used with the grating and prisms is the same. Only a fixed, central portion of the interferogram frame has been used to avoid distortion artifacts from the edges. Moreover, some stray reflection artifacts appearing at the very center of the frames were masked out. The resulting images have been processed with a 1D-FFT performed line by line and the spectra were averaged together. The reported spectra have been normalized against peak value.

The spectra have been also acquired with a reference calibrated dispersive spectrometer (Ocean Optics STS-VIS).

Due to the manufacturing process, the surface qualities of gratings and prisms may vary widely, as discussed in the following Section 5.1.

5. Results

5.1. Roughness measurements

Let's start indicating with $\tilde{S}(x)$ an ideal (the desired one) optical surface, where "x" represents a generic 2D coordinate. Conversely $S(x)$ indicates the real (manufactured) optical surface. Every difference of the real surface profile from the ideal one produces effects from geometrical aberrations to straylight contamination. $E(x) = S(x) - \tilde{S}(x)$ is the surface error and its spectral content, FT(E(x)), can be used to identify different sources of straylight. A first, effective, division can be introduced separating FT(E(x)) into low and high frequencies [25]. Low frequency components produce what is usually referred to as "figure errors" or "waviness"; high frequency components are responsible for finishing or roughness properties. The effects of figure errors can be modelled approximating $\tilde{S}(x)$ with a model accounting for only low frequency content of $\tilde{S}(x)$. Roughness, otherwise, is advantageously studied using statistical models; its effect in broadening the, ideally point-like, sources located at the focal plane of L.S. in Fig. 4 can be studied using the angular resolved scattering technique [26].

The optical surfaces of the grating and prisms have been measured using an atomic force microscope (AFM) (Park Systems XE7 in non-contact mode). In Fig. 6 two representative images of the surface topography of the grating at two different scales are presented; in Fig. 6(a)) and (b) the topographic images at 30μm x 30μm and 2μm x 2μm scale are shown. For both the images, three interesting cuts are highlighted and designated with the letters A, B and C; the corresponding profiles are represented in Figs. 6(c) and (d).

The mean roughness, estimated from scans performed on 2μm x 2μm areas, is 5 nm RMS. Waviness errors can be analyzed looking at the cut "A" in Fig. 6(c)). For better intelligibility, one of the profiles is shown enlarged in Fig. 7. Looking at the profile of three grooves the middle

Optics EXPRESS

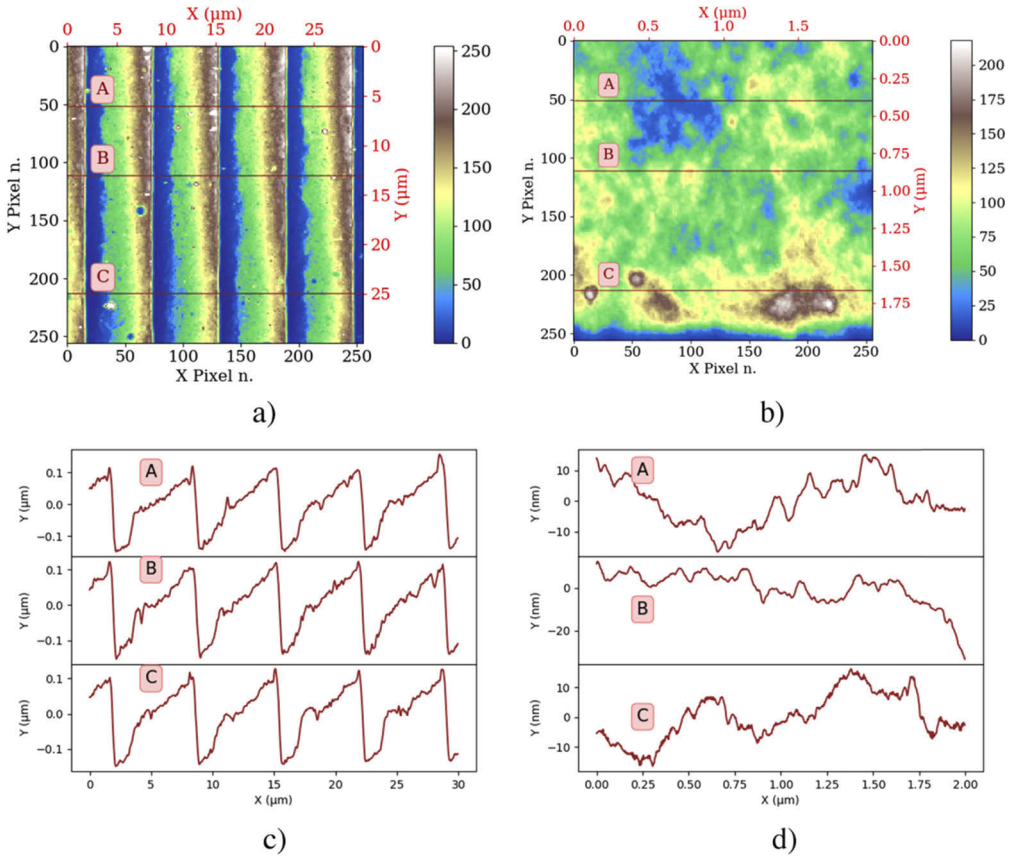

Fig. 6. Surface topography of the grating. a) 30µm x 30µm surface map. b) 2µm x 2µm surface map. c) line profiles of the three cuts in a). d) line profiles of the three cuts in b).

one has a global trend that is close to the nominal 2.13°. On the contrary, the first and last groove have a truncated shape. Both roughness and waviness errors contribute to the stray light.

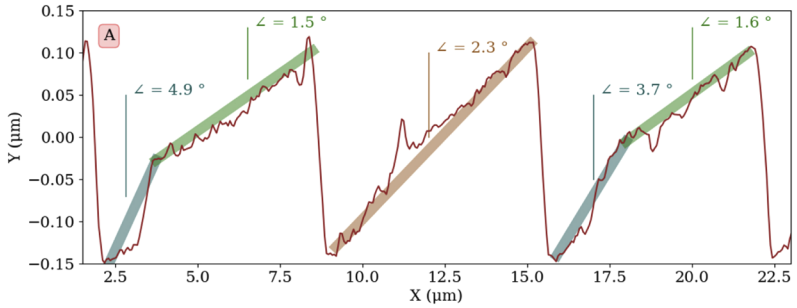

Fig. 7. Profile errors. The image highlights the departure of the real groove's profile from the desired blazed one. The analysis refers to the 'A' profile in Figs. 6(a) and (c).

Prisms have been measured with the same setup used for the grating: the measured roughness is less than the resolving capability of the AFM in the used configuration. Hence, we can conclude that in this case the micro-roughness is less than 0.2 nm. About the waviness, we consider the

Optics EXPRESS

technical specification of the vendor that is of the order of the wavelength. The roughness of the prisms is less than 1/10 compared to that of the gratings. The beneficial effect is straightforward.

From a different perspective: with the same price, commercially available prisms have definitely less roughness than gratings.

The waviness errors act differently in the two compared setups. In the case of prisms, the errors are mapped into wavefront errors and successively into fringes artifacts. In the case of gratings, the smoothed (accounting only for low spatial frequency errors) grooves profile errors produce modifications on the two interfering beams via the diffraction process, and are less intuitive. In this work, this phenomenon is not analyzed, being more focused on roughness effects.

5.2. K spectrum

Figure 8 shows the two interferograms acquired with the two tested configurations using the K lamp. In both cases, the "y" direction is binned by a factor 4, the integration time is 10s and an amplification gain is used in the camera. The non-uniformity in the interferograms is due to stray light contaminations. To reject the out-of-band radiation, an interferential filter (Semrock FF01-550/200-25) coupled with a colored glass (BG family) had been used.

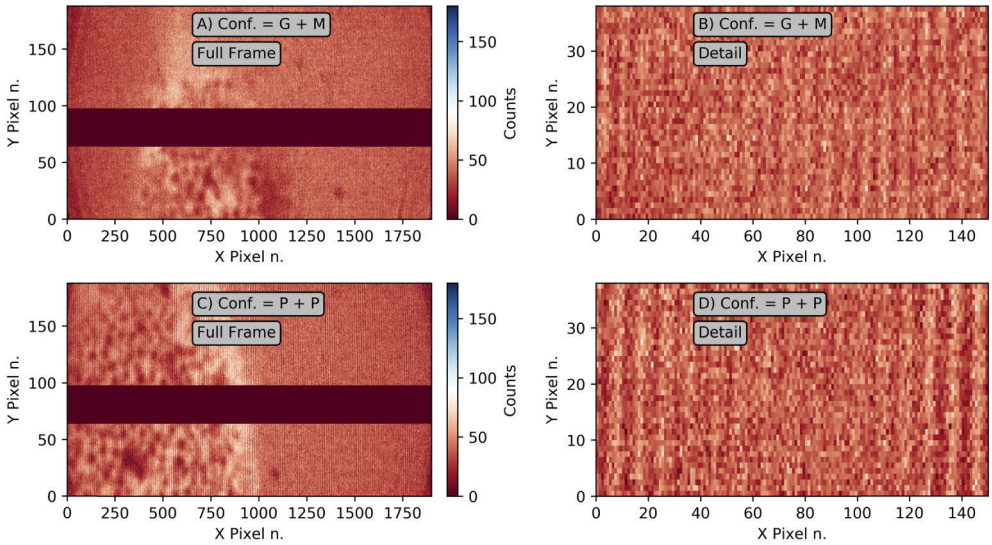

Fig. 8. Potassium lamp interferograms acquired with the grating-based variant (top) and with the prism-based variant (bottom). A) and C) are the full images, B) and D) are details showing the structure of the fringes. The dark band in the center of panel A) and C) is a detector region affected by light interreflection, this region is not considered in the data analysis.

The top panel of Fig. 9 shows the reference spectrum acquired with the reference spectrometer, the mid panel the one produced using the grating configuration and the bottom panel the one produced with the prism-based layout. In all cases, the integration time is 10s. It is quite evident the ability of the prism-based configuration to detect the spectral features of the lamp in the region around 535 nm, while the same spectral features are not observable with the grating-based version.

Being the substitution of the grating/mirror with the two prisms the only change in the configuration, the ability of the proposed configuration of identifying the small spectral features at 535nm is a clear indication of the better S/N of the proposed configuration with respect to the grating-based one.

Optics EXPRESS

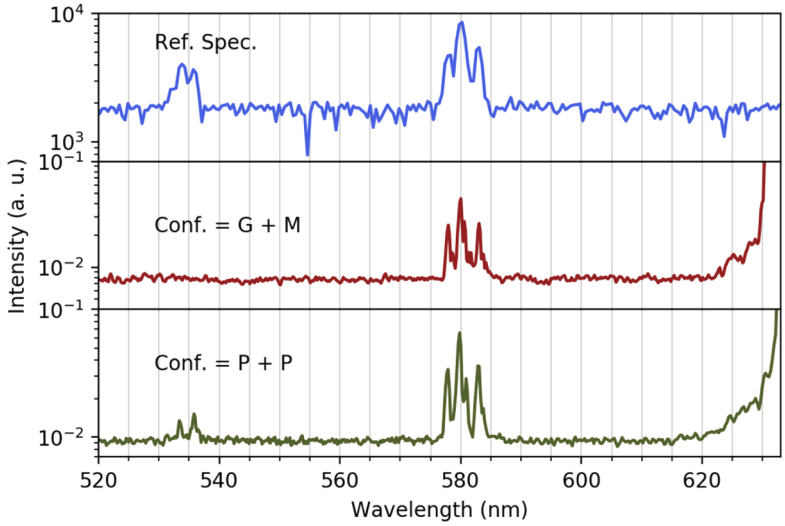

Fig. 9. Potassium lamp spectrum. Comparison between the reference spectrum showing both a weaker band (K lines at 532.328 nm, 533.969 nm, 534.297 nm, 535.957 nm) and a stronger one (K lines at 578.238 nm, 580.175 nm, 581.215 nm, 583.189 nm) (top, blue) with the one acquired with the grating-based version (middle, red) and the one acquired with the prism-based version (bottom, green). Reported line wavelengths are from NIST database; unidentified lines may be visible due to the peculiar gas mixture used by the spectral lamp.

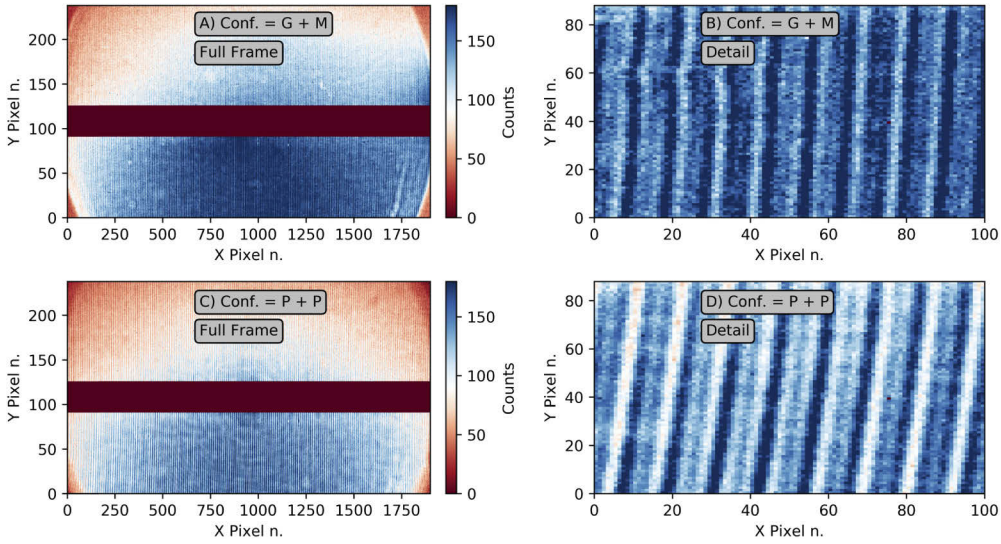

Fig. 10. Krypton lamp interferograms acquired with the grating-based variant (top) and with the prism-based variant (bottom). A) and C) are the full images, B) and D) are details showing the structure of the fringes. The dark band in the center of panel A) and C) is a detector region affected by light interreflection, this region is not considered in the data analysis.

Optics EXPRESS

5.3. Kr spectrum

The two interferograms of the Kr lamp are reported in Fig. 10. As in the previous example, in both cases, the "y" direction is binned by a factor 4, the integration time is 10s and an amplification gain is used in the camera. To reject the out-of-band radiation, an interferential filter (Semrock FF01-550/200-25) has been used. The non-uniformity in the interferograms is due to stray light contaminations.

The comparison between the reconstructed spectra is shown in Fig. 11. In the reference spectrum (top panel, in blue, integration time 12s) the two brightest lines have been saturated with the purpose of evaluating the very faint lines between 598nm and 610nm. Similarly to the previous case, the weak lines are detected using the prism-based configuration, while they are not clearly distinguishable from the noise contribution in the grating-based configuration.

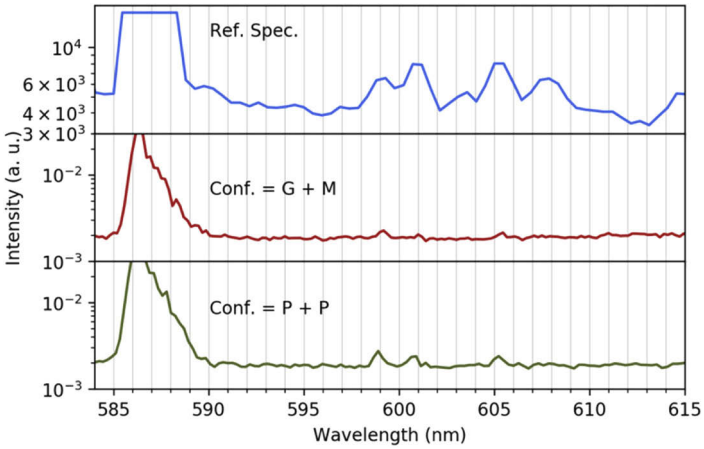

Fig. 11. Krypton lamp spectrum. Comparison between the reference spectrum showing Kr lines at 587.09160 nm, 599.222 nm, 599.38502 nm, 605.61263 nm (top, blue) with the one acquired with the grating-based version (middle, red) and the one acquired with the prism-based version (bottom, green). Reported line wavelengths are from NIST database; unidentified lines may be visible due to the peculiar gas mixture used by the spectral lamp.

6. Conclusions

Static Fourier transform spectrometers (S-FTSs) are well-consolidated instruments providing high throughput and, in the canonic implementation, high-resolution power in a narrow spectral band. The standard configuration uses two reflective gratings as dispersive elements in a Michelson interferometer. We have experimentally demonstrated the beneficial effects on the signal to noise ratio that the substitution of gratings with Littrow prisms produces in a static Fourier transform spectrometer.

From an engineering point of view, a flat surface can be easily polished to higher specification compared to a grating. This suggests that prisms can be valuable components for some high performance SHS applications (astronomical or atmospheric monitoring as example). Another interesting feature of the prisms-based S-FTS is the absence of higher-order reflections, that could enable operation on wider spectral ranges without artifacts in the reconstructed spectra.

Funding. Agenzia Spaziale Italiana (2019-33-HH.0).

Acknowledgments. This work has been supported by ASI agreement n. 2019-33-HH.0.

Disclosures. The authors declare no conflicts of interest.

Optics EXPRESS

References

1. A. Rinnan, F. v. d. Berg, and S. B. Engelsen, "Review of the most common pre-processing techniques for near-infrared spectra," TrAC, Trends Anal. Chem. **28**(10), 1201–1222 (2009).
2. N. D. Lourenço, J. A. Lopes, C. F. Almeida, M. C. Sarraguça, and H. M. Pinheiro, "Bioreactor monitoring with spectroscopy and chemometrics: a review," Anal. Bioanal. Chem. **404**(4), 1211–1237 (2012).
3. A. Pastorello, L. Tartaglia, N. Elias-Rosa, A. Morales-Garoffolo, G. Terreran, S. Taubenberger, U. M. Noebauer, S. Benetti, E. Cappellaro, F. Ciabattari, M. Dennefeld, A. Dimai, E. E. O. Ishida, A. Harutyunyan, S. Leonini, P. Ochner, J. Sollerman, F. Taddia, and S. Zaggia, "Massive stars exploding in a He-rich circumstellar medium – VIII. PSN J07285387 + 3349106, a highly reddened supernova Ibn," Mon. Not. R. Astron. Soc. **454**(4), 4293–4303 (2015).
4. R. J. Dufour, K. B. Kwitter, R. A. Shaw, R. B. C. Henry, B. Balick, and R. L. M. Corradi, "Co-spatial long-slit UV/optical spectra of 10 galactic planetary nebulae with HST/STIS. I. Description of the observations, global emission-line measurements, and CNO abundances," Astrophys. J. **803**(1), 23 (2015).
5. V. Saptari, *Fourier-Transform Spectroscopy Instrumentation Engineering*, (SPIE BOOK, 2003) ISBN: 9780819451644.
6. N. Wiener, "Generalized harmonic analysis," Acta Math. **55**(0), 117–258 (1930).
7. A. Khintchine, "Korrelationstheorie der stationären stochastischen Prozesse," Math. Ann. **109**(1), 604–615 (1934).
8. P. R. Griffiths and J. A. De Haseth, *Fourier Transform Infrared Spectrometry* (Wiley, 2007) ISBN: 978-0-471-19404-0.
9. B.C. Smith, *Fundamentals of Fourier Transform Infrared Spectroscopy* (CRC, 2011) ISBN: 978-1420069297.
10. P. Connes, "Spectromètre interférentiel a sélection par l'amplitude de modulation (1)," J. Phys. Radium **19**(3), 215–222 (1958).
11. P. Jacquinot, "New developments in interference spectroscopy," Rep. Prog. Phys. **23**(1), 267–312 (1960).
12. F. L. Roesler and J. M. Harlander, "Spatial heterodyne spectroscopy: interferometric performance at any wavelength without scanning," *Proc. SPIE* 1318, (1990).
13. J. Harlander, R. J. Reynolds, and F. L. Roesler, "Spatial Heterodyne Spectroscopy for the Exploration of Diffuse Interstellar Emission Lines at Far-Ultraviolet Wavelengths," Astrophys. J. **396**, 730 (1992).
14. C. R. Englert, J. M. Harlander, C. M. Brown, and K. D. Marr, "Spatial heterodyne spectroscopy at the Naval Research Laboratory," Appl. Opt. **54**(31), F158–F163 (2015).
15. M. Lenzner and J.-C. Diels, "Concerning the Spatial Heterodyne Spectrometer," Opt. Express **24**(2), 1829–1839 (2016).
16. J. M. Harlander, F. L. Roesler, J. G. Cardon, C. R. Englert, and R. R. Conway, "SHIMMER: a spatial heterodyne spectrometer for remote sensing of Earth's middle atmosphere," Appl. Opt. **41**(7), 1343–1352 (2002).
17. W. M. Harris, F. L. Roesler, J. Harlander, L. Ben-Jaffel, E. Mierkiewicz, J. Corliss, and R. J. Oliversen, "Applications of reflective spatial heterodyne spectroscopy to UV exploration in the solar system," Proc. SPIE **5488**, 886–897 (2004).
18. M. Heusinger, D. Michaelis, T. Flügel-Paul, and U. Zeitner, "Diffuse scattering due to stochastic disturbances of 1D-gratings on the example of line edge roughness," Opt. Express **26**(21), 28104–28118 (2018).
19. J. Rochester and A. Martin, "Improving the Performance of a Littrow-type Infra-Red Spectrometer," Nature **168**(4279), 785–786 (1951).
20. C. N. Pannell, B. G. Zhang, and M. K. Reed, "The spatially heterodyned spectrometer: A for high resolution Raman spectroscopy?" Proc. SPIE **9369**, 936903 (2015).
21. M. J. Padgett and A. R. Harvey, "A static Fourier-transform spectrometer based on Wollaston prisms," Rev. Sci. Instrum. **66**(4), 2807–2811 (1995).
22. D. Komisarek, K. Reichard, and S. Yin, "Enhancing the performance of non-scanning Fourier transform spectrometer by compensating manufacturing defects inherent to a Wollaston prism array," Opt. Commun. **238**(1-3), 85–90 (2004).
23. J. Courtial, B. Patterson, A. Harvey, W. Sibbett, and M. Padgett, "Design of a static Fourier-transform spectrometer with increased field of view," Appl. Opt. **35**(34), 6698–6702 (1996).
24. M. Schardt, P. Murr, M. Rauscher, A. Tremmel, B. Wiesent, and A. Koch, "Static Fourier transform infrared spectrometer," Opt. Express **24**(7), 7767–7776 (2016).
25. J. E. Harvey, N. Choi, S. Schroeder, and A. Duparré, "Total integrated scatter from surfaces with arbitrary roughness, correlation widths, and incident angles," Opt. Eng. **51**(1), 013402 (2012).
26. S. Schröder, A. Duparré, L. Coriand, A. Tünnermann, D. H. Penalver, and J. E. Harvey, "Modeling of light scattering in different regimes of surface roughness," Opt. Express **19**(10), 9820–9835 (2011).